

Cite this: *Dalton Trans.*, 2016, **45**,  
3506

## Synthesis and characterization of DNA fenced, self-assembled SnO<sub>2</sub> nano-assemblies for supercapacitor applications

U Nithiyantham,<sup>a</sup> Ananthakumar Ramadoss<sup>b</sup> and Subrata Kundu\*<sup>a</sup>

Self-assembled, aggregated, chain-like SnO<sub>2</sub> nano-assemblies were synthesized at room temperature by a simple wet chemical route within an hour in the presence of DNA as a scaffold. The average size of the SnO<sub>2</sub> particles and the chain diameter were controlled by tuning the DNA to Sn(II) molar ratio and altering the other reaction parameters. A formation and growth mechanism of the SnO<sub>2</sub> NPs on DNA is discussed. The SnO<sub>2</sub> chain-like assemblies were utilized as potential anode materials in an electrochemical supercapacitor. From the supercapacitor study, it was found that the SnO<sub>2</sub> nanomaterials showed different specific capacitance ( $C_s$ ) values depending on varying chain-like morphologies and the order of  $C_s$  values was: chain-like (small size) > chain-like (large size). The highest  $C_s$  of 209 F g<sup>-1</sup> at a scan rate of 5 mV s<sup>-1</sup> was observed for SnO<sub>2</sub> nano-assemblies having chain-like structure with a smaller size. The long term cycling stability study of a chain-like SnO<sub>2</sub> electrode was found to be stable and retained ca. 71% of the initial specific capacitance, even after 5000 cycles. A supercapacitor study revealed that both morphologies can be used as a potential anode material and the best efficiency was observed for small sized chain-like morphology which is due to their higher BET surface area and specific structural orientation. The proposed route, by virtue of its simplicity and being environmentally benign, might become a future promising candidate for further processing, assembly, and practical application of other oxide based nanostructure materials.

Received 17th December 2015,  
Accepted 6th January 2016

DOI: 10.1039/c5dt04920b

www.rsc.org/dalton

## Introduction

In recent years, interest in the fabrication of one-dimensional (1-D) semiconductor materials has attracted great research attention because of their potential importance in fundamental research and in technological perspectives. Considerable attention has been made to construct 1D semiconducting materials using a variety of nanofabrication techniques and crystal growth mechanisms. Template-based synthesis of 1-D nano-assemblies is an elegant chemical approach for the fabrication of nanostructures.<sup>1,2</sup> At nanoscale, materials show intrinsic properties that are governed by their size, shape, and structures. Careful literature investigation revealed that the study of metal nanomaterials is more comparable to semiconductor metal oxides. Hence, considerable attention has been devoted to a 'bottom-up' method where molecular components are self-assembled into a complex structure. Therefore, it is quite reasonable to determine a suitable route for the syn-

thesis of 1-D self-assembled nanomaterials in a short time scale and in an easy manner. Among the different oxide materials studied so far, tin dioxide (SnO<sub>2</sub>), particularly was found to be more interesting and have many important applications.<sup>3–8</sup> SnO<sub>2</sub> is a n-type semiconductor with a large band gap ( $E_g = 3.6$  eV at 300 K), which finds wide application in gas sensors,<sup>3</sup> dye sensitized solar cells (DSSC),<sup>4,5</sup> catalysis reactions,<sup>6</sup> Li-ion batteries,<sup>7</sup> and as a suitable electrode material in electrochemical supercapacitors.<sup>8</sup>

Different morphologies of low dimensional SnO<sub>2</sub> nanostructures have been reported (like zero dimensional nanoparticles (NPs),<sup>9</sup> 1-D nanorods,<sup>10</sup> nanobelts,<sup>11</sup> nanowires,<sup>12</sup> nanotubes,<sup>13</sup> and two-dimensional (2-D) nanosheets<sup>14</sup>). Moreover, recently a three-dimensional (3-D) hierarchical architecture has also been reported by a few researchers.<sup>15,16</sup> Additionally, doping of SnO<sub>2</sub> based nanomaterials offers a convenient way to tailor their electrical, structural, and optical properties. Therefore, development of suitable synthetic strategies is crucial for providing desired property control. Different types of bio-molecules such as proteins, peptides, and amino acids can be used as scaffolds, templates, and stabilizers for the formation of metal, hybrid, and composite nanomaterials with unique properties.<sup>17–19</sup> Among the different bio-molecules, deoxyribonucleic acid (DNA) has been used widely as a biological template to build nanostructures with specific

<sup>a</sup>Electrochemical Materials Science (ECMS) Division, CSIR-Central Electrochemical Research Institute (CECRI), Karaikudi 630006, Tamil Nadu, India.

E-mail: skundu@cecri.res.in, subrata\_kundu2004@yahoo.co.in;

Fax: +91-4565-227651; Tel: +91-4565-241487

<sup>b</sup>School of Electrical Engineering, Korea Advanced Institute of Science and Technology (KAIST), 291 Daehak-ro, Yuseong-gu, Daejeon, 305-701, South Korea



morphologies.<sup>20,21</sup> DNA strands offered a variety of binding sites for several metal ions and stands to be an ideal candidate for programming the self-assembly of nanomaterials into 1-D structures.<sup>22–24</sup> In DNA structures, mainly two binding sites are available. The first one is the negatively charged phosphate group and another one is the aromatic base molecules. A few other important properties of DNA are: (i) a double helix structure with better mechanical strength; (ii) intermolecular interactions in DNA can be readily programmed and reliably predicted; and (iii) the versatile chemical structure allowed DNA to self-assemble into complex structure-like cubes, squares, *etc.*<sup>25–28</sup> The backbone of DNA, made of phosphate and sugar molecules, can bind with various metal cations and metal NPs *via* electrostatic interactions. Therefore, within the past few years, a growing number of researchers have been paying attention to using DNA as “smart materials” to direct the assembly of inorganic materials.

As discussed before, SnO<sub>2</sub> nanomaterials can be used widely in DSSC and as electrode materials in electrochemical supercapacitor studies.<sup>4,5,7,8</sup> It is well-known that SnO<sub>2</sub> acquires a special place because of its lower cost and environmentally benign nature. Similarly, different oxide materials like MnO<sub>2</sub>,<sup>29</sup> TiO<sub>2</sub>,<sup>30</sup> and RuO<sub>2</sub><sup>31</sup> have been used as electrode materials for supercapacitors because of their large capacitance and fast redox kinetics. However, to reduce the cost factor, alternative oxides were investigated. A SnO<sub>2</sub> composite with polyaniline (PANI) showed good supercapacitive activity.

Different routes have been employed for the synthesis of SnO<sub>2</sub> nanomaterials. Sunkara *et al.* synthesized SnO<sub>2</sub> nanowires on a quartz substrate and observed a DSSC efficiency of 2.1%.<sup>32</sup> Qiao *et al.* prepared an urchin-like SnO<sub>2</sub> microstructure and coated it with thin layers of TiO<sub>2</sub> for their application in DSSC.<sup>33</sup> Zhang *et al.* prepared a PANI–SnO<sub>2</sub> composite for supercapacitor applications.<sup>34</sup> Wang *et al.* prepared single crystalline SnO<sub>2</sub> nanorod arrays using hydrothermal routes and observed a DSSC efficiency <0.4%.<sup>35</sup> Xie *et al.* prepared SnO<sub>2</sub> nanotubes and SnO<sub>2</sub>–TiO<sub>2</sub> core shell nanomaterials for DSSC applications.<sup>36</sup> They observed that bare SnO<sub>2</sub> gave efficiency ~0.99% whereas SnO<sub>2</sub>–TiO<sub>2</sub> composites gave efficiency of 5.11%. Tremel *et al.* synthesized SnO<sub>2</sub> nanocrystals by a microwave-based hydrothermal route and used them in DSSC applications.<sup>37</sup> There are a few other reports where SnO<sub>2</sub> nanomaterials were synthesized using different routes and then applied as a battery material or in a photocatalytic reaction.<sup>38,39</sup> Most of the above reports on SnO<sub>2</sub> nanomaterials required a long reaction time, high temperature, very expensive reagents, or generated particles with various morphologies. So, we investigated an easy route with a low temperature reaction and uniform particle morphology for the synthesis of SnO<sub>2</sub> nanomaterials. To the best of our knowledge, there is no information available for the formation of aggregated, chain-like SnO<sub>2</sub> nano-assemblies on a DNA scaffold within 1 h of reaction time at room temperature. The chain-like SnO<sub>2</sub> nano-assemblies on DNA show potential applications in electrochemical supercapacitors and in DSSC studies.

In this article we synthesized aggregated, chain-like SnO<sub>2</sub> nano-assemblies on a DNA scaffold at room temperature with 40 min of reaction time. SnO<sub>2</sub> nano-chains were synthesized by the reaction of SnCl<sub>2</sub> and water in the presence of DNA under continuous stirring. The small size SnO<sub>2</sub> particles are self-assembled, aggregated, and grown on DNA with a chain-like morphology. The size of the individual SnO<sub>2</sub> particles, diameter, and length of the chains was tuned by altering the DNA with SnCl<sub>2</sub> molar ratio and controlling other reaction parameters. The SnO<sub>2</sub> chain-like assemblies were utilized as potential anode materials in electrochemical supercapacitors. From electrochemical supercapacitor studies, it was found that SnO<sub>2</sub> nano-assemblies showed different specific capacitance ( $C_s$ ) values for various nano-chains and the order of  $C_s$  values were as follows: chain-like (small size) > chain-like (large size). A long term cycling stability study of a chain-like SnO<sub>2</sub> electrode showed it to be stable and retaining a  $C_s$  value 71% of its initial specific capacitance, even after 5000 consecutive cycles. The supercapacitor study revealed that both of the morphologies can be used as a potential anode material and the best efficiency was observed for small size chain-like morphology which is due to their higher BET surface area and specific structural orientation. In the future, the proposed route, by virtue of its simplicity and being environmentally benign, might become a promising candidate for further processing, assemblies, and practical applications for other oxide-based nanostructure materials.

## Experimental section

### Reagents

DNA (double-stranded herring testes) with an average molecular weight ~50 K bp (base pair) was purchased from Sigma-Aldrich. The Sn(II) chloride (SnCl<sub>2</sub>) salt was obtained from Sigma-Aldrich and used as received. Absolute ethyl alcohol (CH<sub>3</sub>CH<sub>2</sub>OH) was obtained from Changshu Yangyuan Chemical from China. *N*-Methyl-2-pyrrolidone (NMP), acetylene black was purchased from Sigma-Aldrich and used as received. Nickel foam and polyvinylidene fluoride (PVDF) were obtained from Alfa Aesar. De-ionized (DI) water was used for the entire synthesis and application purposes.

### Instruments

The synthesized chain-like SnO<sub>2</sub> nano-assemblies on DNA scaffolds were characterized using several spectroscopic techniques. Transmission electron microscopy (TEM) and high resolution transmission electron microscopy (HR-TEM) analysis was done with a Tecnai model TEM instrument (TecnaiTM G2 F20, FEI) with an accelerating voltage of 200 KV. The UV-Visible (UV-Vis) absorption spectra were recorded with a Unico (model 4802) UV-Vis-NIR spectrophotometer equipped with a 1 cm quartz cuvette holder for liquid samples. Energy Dispersive X-ray Spectroscopy (EDS) analysis was done with a Field Emission Scanning Electron Microscopy (FE-SEM) instrument (Zeiss ultra FE-SEM instruments) with a separate EDS



detector (INCA) connected to it. X-ray diffraction (XRD) analysis was done using a PAN analytical Advanced Bragg-Brentano X-ray powder diffractometer (XRD) with Cu K $\alpha$  radiation ( $\lambda = 0.154$  nm) with a scanning rate of 7 degree per min in the  $2\theta$  range 10–90°. The photoluminescence (PL) study was done with a Varian (Cary Eclipse Winflr) fluorescence spectrophotometer (serial number e102045776), both in excitation and emission modes, using a xenon pump lamp. Fourier Transform Infrared (FT-IR) spectroscopy analysis was done with the model Nexus 670 (FTIR), Centaurus 10 $\times$  (Microscope) having a spectral Range of 4000 to 400  $\text{cm}^{-1}$  with a MCT-B detector. The thermal analysis study was recorded with a thermal analyser-simultaneous TGA/DTA instrument with model name SDT Q600 and the analysis was performed in air. A hot air oven (temperature up to 1000 °C) was used to anneal the samples at a specific temperature. All the electrochemical experiments were examined using an AUTOLAB PGSTAT302N electrochemical work station in a 2 M KOH aqueous solution.

### Synthesis of self-assembled, aggregated chain-like SnO<sub>2</sub> nano-assemblies on DNA scaffold

SnO<sub>2</sub> nano-assemblies having a chain-like morphology can be synthesized by the reaction of SnCl<sub>2</sub> aqueous salt solution in the presence of DNA under continuous stirring. For a typical synthesis, 10 mL of DNA solution was mixed with 130 mL of water and stirred for 10 minutes. The solution was colorless at that stage. Next, 200 mL of 0.5(M) Sn(II) salt solution was added drop wise for 10 min with continuous stirring. The colorless solution slowly turned into a milky white turbid solution. The solution was continuously stirred for another 20 min. After 5–10 min, a white sediment settled and it was collected by centrifugation with water and ethanol for 3–4 times. After centrifugation, the white paste-like Sn(OH)<sub>2</sub> was heated initially at 60 °C for 1 h and finally annealed at 600 °C for 3 h. The other sets were prepared by varying the concentration of the starting reagents. Table 1 shows different final concentrations of all the reagents used for the synthesis, total time of reaction, size of the materials, and shape of the particles. Scheme 1 is a schematic representation of the entire synthesis process.

### Fabrication of electrodes for electrochemical supercapacitor applications

A working electrode was prepared by mixing the electroactive material, acetylene black and polyvinylidene fluoride (PVDF) with a mass ratio of 80 : 10 : 10 in *N*-methyl-2-pyrrolidone to

form a homogeneous slurry. Then the slurry was coated on the nickel foam current collector (area = 1 cm  $\times$  1 cm) and dried at 90 °C for 24 h to evaporate the solvent. The loading mass of the electroactive material was about 7 mg  $\text{cm}^{-2}$ . Electrochemical measurements were carried out using a standard three electrode system with 2 M KOH aqueous solution. A platinum sheet and Hg/HgO were used as the counter and reference electrode, respectively. Cyclic voltammetry (CV) tests were performed at various scan rates within a potential range of 0 to 0.6 V. Galvanostatic charge–discharge (CD) measurements were carried out in the potential range from 0 to 0.55 V at a current density of 0.5, 1, 2, 3, 4, 5, and 7.5 A  $\text{g}^{-1}$ . Electrochemical impedance spectroscopy (EIS) tests were conducted over the frequency range of 100 kHz to 10 mHz with an AC amplitude of 5 mV at open circuit potential. The specific capacitances of the SnO<sub>2</sub> electrodes were calculated from the CV and GCD curves, according to the following equations:<sup>29,40</sup>

$$C_s = \frac{\int idV}{2vm\Delta V} \quad (1)$$

$$C_s = \frac{I\Delta t}{m\Delta V} \quad (2)$$

where,  $C_s$  is the specific capacitance ( $\text{F g}^{-1}$ ),  $\int idV$  is the integrated area under the CV curve (A),  $v$  is the scan rate ( $\text{mV s}^{-1}$ ),  $m$  is the mass of the electroactive material (g),  $\Delta V$  is the potential window (V),  $I$  is the discharge current (A), and  $\Delta t$  is the discharge time (s).

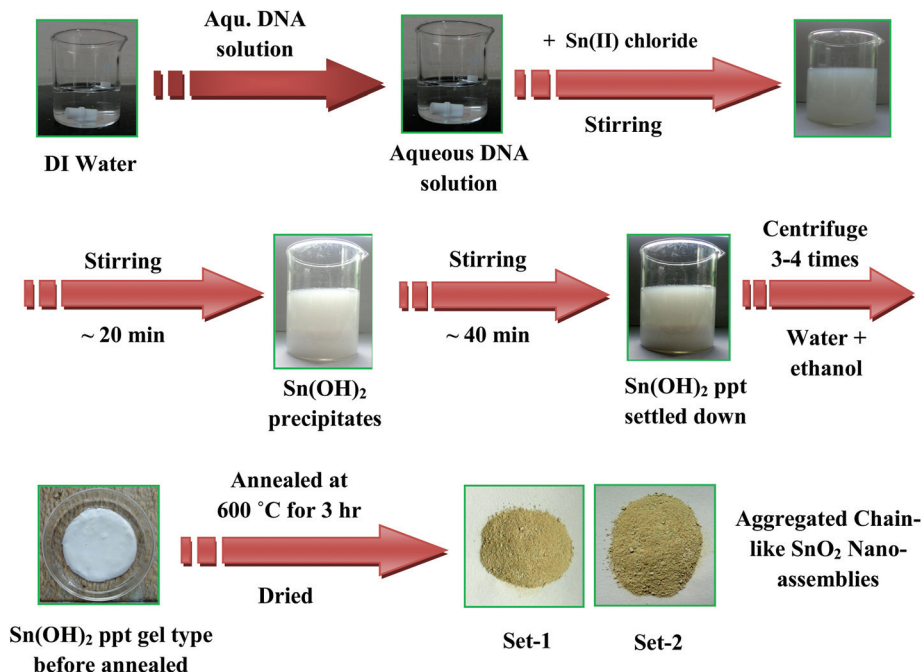
### Preparation of samples for different other characterizations

The chain-like SnO<sub>2</sub> nano-assemblies on a DNA scaffold were characterized using UV-Vis, TEM, EDS, XRD, photoluminescence (PL), LASER-Raman, FT-IR, and thermal analysis. The SnO<sub>2</sub> nano-assemblies solution, after successive centrifugation and annealing, was used for measurements in a UV-Vis spectrophotometer after dispersing in an aqueous solution. The solid SnO<sub>2</sub> powder was mixed with DI water, sonicated for 20 min and used for TEM sample preparation and other thin film preparations. The dispersed SnO<sub>2</sub> nanostructures in aqueous solution were used for the PL measurements. Samples for TEM were prepared by placing a drop of the corresponding SnO<sub>2</sub> NPs solution onto a carbon coated Cu grid followed by slow evaporation of solvent at ambient conditions. For EDS, XRD, Laser Raman, and FT-IR analysis, glass slides were used as substrates for thin film preparation. The slides were cleaned thoroughly in acetone and sonicated for

**Table 1** The different final concentrations of all reagents used, size and shape of the particles for the formation of self-assembled, aggregated, chain-like SnO<sub>2</sub> nano-assemblies on DNA

Set no.	Final conc. of DNA (M)	Final conc. of SnCl <sub>2</sub> salt (M)	Volume of DI water added (mL)	Total time of stirring at RT (min)	Shape of the SnO <sub>2</sub> nano-assemblies	Approx. size of the SnO <sub>2</sub> particles (nm)	Shape distribution
1	$3.61 \times 10^{-3}$	$2.94 \times 10^{-2}$	130	40	Aggregated chain-like	Chain diameter $40 \pm 5$ , individual NPs size $\sim 3.5 \pm 0.2$	100% chain-like
2	$5.06 \times 10^{-2}$	$2.94 \times 10^{-2}$	0	40	Aggregated chain-like	Chain diameter $100 \pm 10$ , individual NPs size $\sim 2.0 \pm 0.3$	100% chain-like





**Scheme 1** Shows the schematic presentation for the synthesis of DNA–SnO<sub>2</sub> nano-assemblies.

about 20 min. The cleaned substrates were covered with the SnO<sub>2</sub> nanostructures solution and then dried in air. After the first layer was deposited, subsequent layers were deposited by repeatedly adding more SnO<sub>2</sub> nanostructures solution and drying. Final samples were obtained after 5–6 times depositions and then analyzed using the above techniques. For TGA/DTA analysis, the as prepared DNA–SnO<sub>2</sub> nano powders were directly used for the measurements. The sample preparation for a supercapacitor application is given in a later section under the experimental part.

## Results and discussion

### UV-Vis spectroscopic study

Fig. 1A shows the room temperature UV-Visible (UV-Vis) spectra of different solution mixtures for the formation of self-assembled chain-like SnO<sub>2</sub> nano-assemblies on a DNA scaffold. Curve a, Fig. 1A shows the absorption band of only aqueous DNA solution which has a peak maxima at 258 nm due to absorption of aromatic base molecules. Curve b (Fig. 1A) shows the absorption band of only aqueous Sn(II) chloride solution and an absorption hump near 282 nm is observed due to ligand to metal charge transfer (LMCT) spectra. Similar types of LMCT bands were observed for other metal salts like Au and Mn.<sup>21,29</sup> Fig. 1A, curve c shows the absorption band of a mixture of aqueous DNA and aqueous Sn(II) salt, where the absorption hump of Sn(II) salt is not visible although the DNA peak is observed with few nm shifts than the original position. This is due to absorption of oppositely charged Sn<sup>+2</sup> ions in DNA. Curve d and e in Fig. 1A show the

excitonic absorption band of SnO<sub>2</sub> for chain-like (large size) and chain like (small size) nano-assemblies, respectively. From both spectra, we observed a strong peak and, in addition, a small absorption hump at a lower wavelength side below 300 nm. Similar types of UV-Vis absorption bands were observed earlier by Yuan *et al.*<sup>41</sup> and Han *et al.*<sup>42</sup> from their studies on SnO<sub>2</sub> nanomaterials. Shifting of absorption hump position for both the morphologies is probably due to the change in particle diameter as discussed in the TEM and FE-SEM analysis section below. Apart from this, we also measured the excitonic transition of SnO<sub>2</sub> samples to calculate the band gap energies as shown in Fig. 1B. The theoretical expression determination of band gap *via* Tauc plot is given elsewhere.<sup>43</sup> From the mathematical expression in the Tauc equation, a plot of  $(\alpha E_p)^2$  versus  $E_p$  based on a direct transition and the extrapolated value of  $E_p$  at  $\alpha = 0$  gives the band gap of SnO<sub>2</sub> particles. In the equation  $\alpha$  is the absorption coefficient and  $E_p$  is the direct photo energy. Curve a and curve b in Fig. 1B show the spectra of SnO<sub>2</sub> chain-like morphology having (large size) and SnO<sub>2</sub> chain-like morphology having (small size), respectively. The calculated band gap for two different morphologies was 3.46 eV and 3.98 eV, respectively. Compared with the band gap energy of 3.6 eV of SnO<sub>2</sub> powder at room temperature, the near band absorption for the SnO<sub>2</sub> chain-like nano-assemblies exhibits a blue shift as well as a red shift for the two different morphologies which is ascribed to the size effect of the nanocrystals as reported by others.<sup>42</sup> Considering the blue shift and red shift of the two different morphologies compared to bulk SnO<sub>2</sub> (band gap  $\sim$ 3.6 eV), the absorption onset of the synthesis materials can be assigned to the direct transition of electrons in SnO<sub>2</sub> nanomaterials.



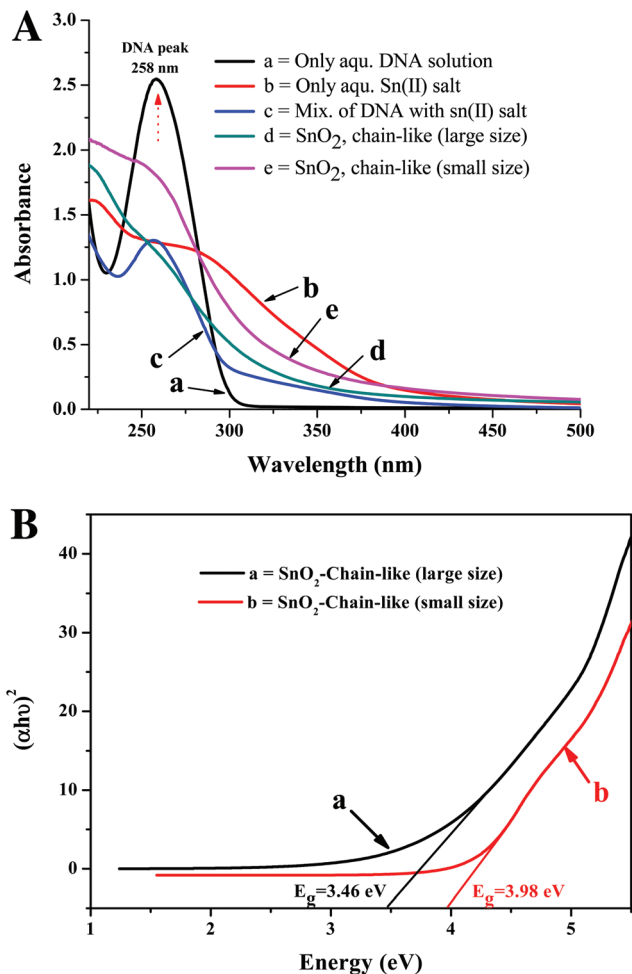


**Fig. 1** (A) UV-Visible (UV-Vis) absorption spectra of different solution mixtures for the synthesis of self-assembled, aggregated, chain-like SnO<sub>2</sub> nano-assemblies on a DNA scaffold. Curve a shows the absorption spectra of only aqueous DNA solution; curve b shows the absorption band of only aqueous Sn(II) chloride solution; curve c shows the absorption spectrum of the mixture of tin(II) chloride solution with the aqueous DNA solution; curves d and e show the absorption bands of chain-like SnO<sub>2</sub> nano-assemblies on DNA with larger and smaller sizes of individual particles respectively. (B) The excitonic transition of SnO<sub>2</sub> samples to calculate the band gap energies of chain-like SnO<sub>2</sub> nano-assemblies for large size (curve a) and small size (curve b), respectively.

### Transmission electron microscopy (TEM) and field-emission scanning electron microscopy (FE-SEM) analysis

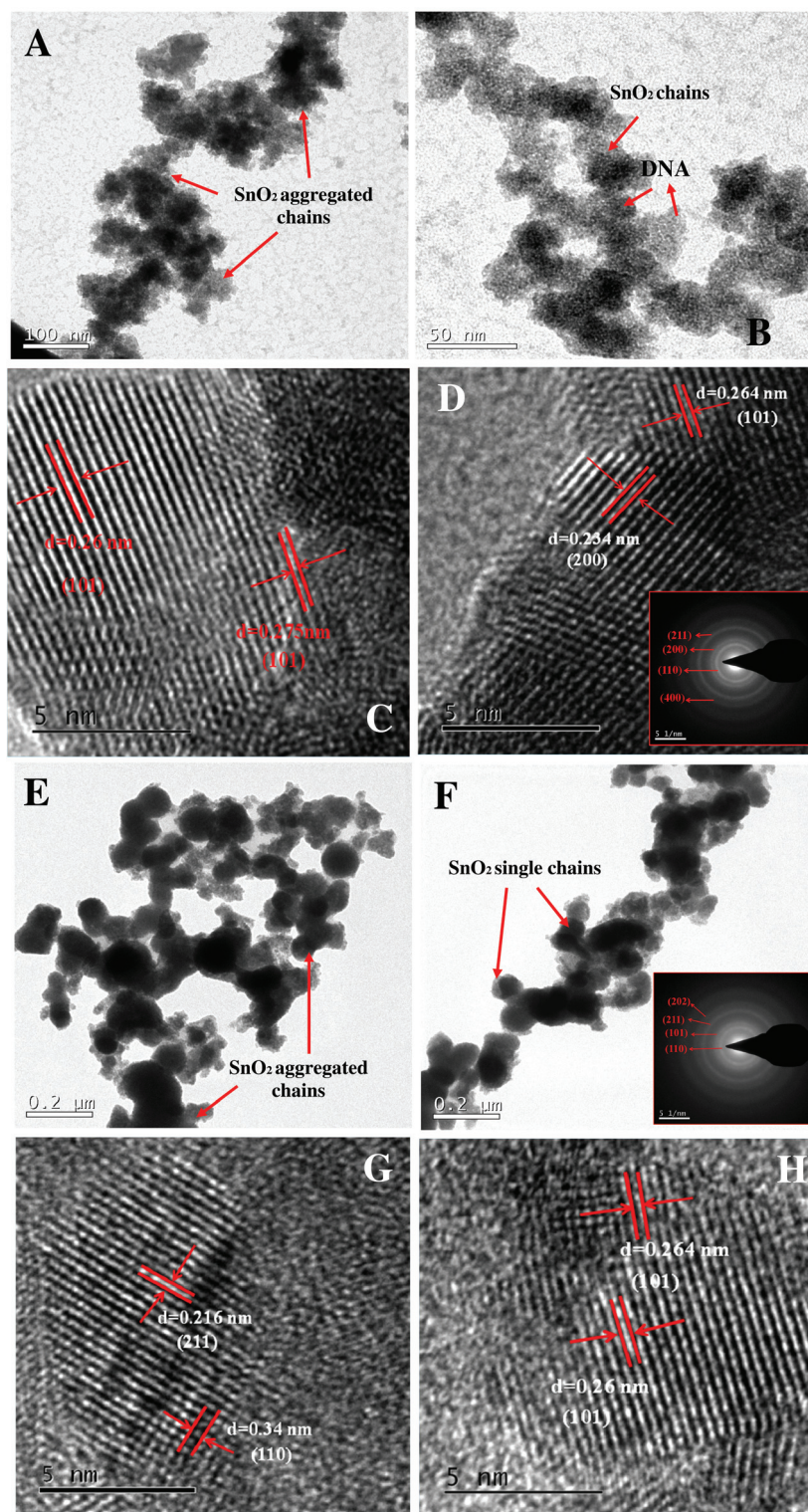
Transmission Electron Microscopy (TEM) images of the chain-like SnO<sub>2</sub> nano-assemblies are shown in Fig. 2. Fig. 2A–D shows the low and high magnified images of the chain-like SnO<sub>2</sub> nano-assemblies on DNA having larger sizes. From the images, the average sizes of the individual SnO<sub>2</sub> particle are  $\sim 3.5 \pm 0.2$  nm. The nominal lengths of the chains are  $\sim 1$ – $2$   $\mu\text{m}$ . The average chain diameters are  $\sim 40 \pm 5$  nm. Fig. 2C and D shows the high resolution transmission electron microscopy (HR-TEM) images where lattice fringes are clearly visible. In Fig. 2C, the lattice spacing ( $d$ ) are 0.26 nm and 0.275 nm and both arise from the (101) lattice plane. Similarly,

in Fig. 2D, there are two types of fringes visible where the lattice spacing ( $d$ ) is 0.264 nm (for 101 plane) and 0.234 nm (for 200 plane), respectively. The inset of Fig. 2D shows the corresponding selected area electron diffraction (SAED) pattern where we did not observe any separate spots either due to small size of the particles or due to their nanocrystalline nature. The ring-type pattern is indexed as (110), (202), (211), and (400) crystal planes of SnO<sub>2</sub> nanomaterials. Fig. 2E–H shows the low and high magnified TEM images of the chain-like SnO<sub>2</sub> nano-assemblies on a DNA scaffold with small sized particles. Fig. 2E and F is the low magnification image where many chains are assembled to form a network structure (Fig. 2E) and the image of a single nano-chain structure (Fig. 2F). The average individual particles size is calculated to be  $\sim 2.0 \pm 0.3$  nm whereas the nominal lengths of the chains are  $\sim 1.5$ – $2.5$   $\mu\text{m}$ . The average diameters of the chains are  $\sim 100 \pm 10$  nm. From the image, it is clear that small sized particles are aggregated together to form the chain-like structures. Fig. 2G and H shows the HR-TEM images where lattice fringes are clearly visible. In Fig. 2G, two different crystal planes are visible where the lattice spacing ( $d$ ) is 0.216 nm (for 211 plane) and 0.34 nm (for 110 plane) respectively. Similarly, in Fig. 2H, there is one type of fringe visible where the lattice spacing ( $d$ ) is 0.264 nm and arises from the 101 plane. The inset of Fig. 2F shows the corresponding SAED pattern which indicates the particles are crystalline in nature. Although, due to the very small size of the individual particles, we did not observe separate diffraction spots like with single crystal nanomaterials. The ring-type pattern is indexed as (110), (101), (211), and (202) crystal planes of SnO<sub>2</sub> nanomaterials. The presence of DNA is visible from all the TEM images and it is clear that the small size SnO<sub>2</sub> nano-assemblies are formed initially, then they grow on the DNA chain, aggregate together and generate the chain-like morphologies. Fig. 3A–D shows the FE-SEM images of the chain-like SnO<sub>2</sub> nano-assemblies for the different morphologies. Images A–B show the large size SnO<sub>2</sub> nano-assemblies at low and high magnification. From the low magnified image it is clear that the formation has an aggregated chain-like morphology and from the high magnified image it is clear that the small particles are assembling together to form the chain-like morphology. The average diameter of the particles and the nominal length of the chains match with the TEM analysis in Fig. 2. Similarly, Fig. 3, image C–D shows the FE-SEM image of the SnO<sub>2</sub> chain-like nano-assemblies having smaller sizes. The average size of the SnO<sub>2</sub> particles in the nano-chain morphology match with the TEM results as discussed earlier. Therefore, both from TEM and FE-SEM analyses, it is clear that small size SnO<sub>2</sub> particles were formed initially, grew on the DNA chain, and then aggregated and self-assembled together and generated the chain-like morphology.

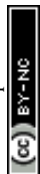
### Energy dispersive X-ray spectroscopy (EDS) and X-ray diffraction (XRD) analysis

The energy dispersive X-ray spectroscopic (EDS) analysis of the synthesized DNA–SnO<sub>2</sub> nanomaterials is shown in Fig. 4A. The EDS spectrum consists of the different peaks for Sn, Cl, P, O,





**Fig. 2** Transmission electron microscopy (TEM) images of the chain-like  $\text{SnO}_2$  nano-assemblies on a DNA scaffold. A–D show the low and high magnified TEM images having larger size  $\text{SnO}_2$  nano-assemblies; the inset of D shows the corresponding selected area electron diffraction (SAED) pattern. E–H show the low and high magnified TEM images of the small size  $\text{SnO}_2$  nano-assemblies; the inset of F shows the corresponding SAED pattern.



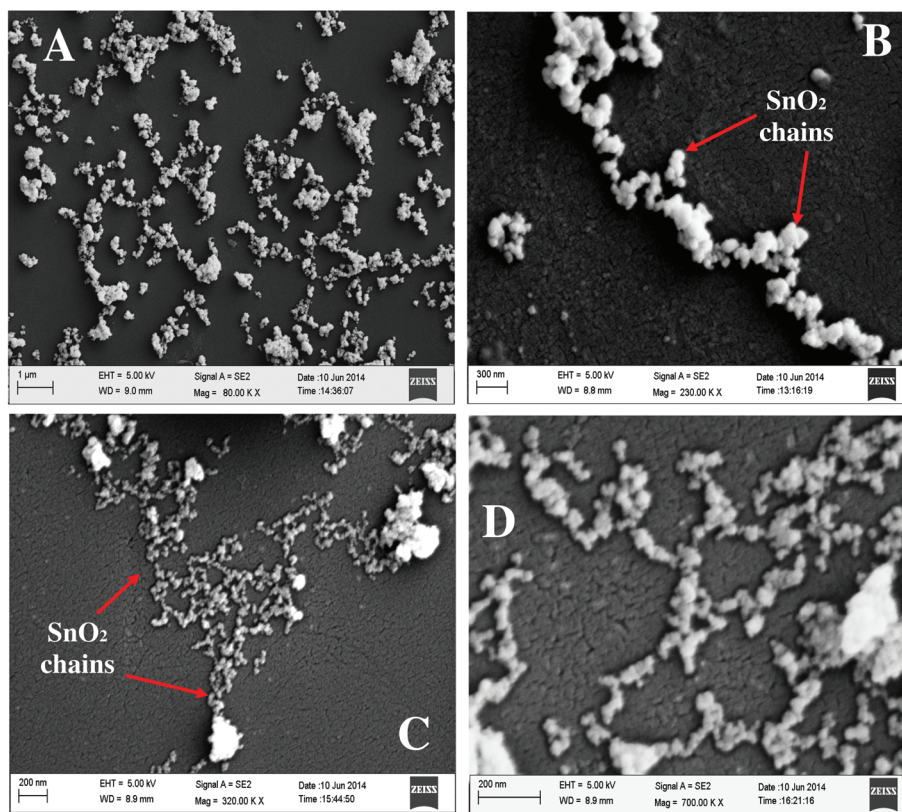


Fig. 3 Low and high magnified FE-SEM images of the large size SnO<sub>2</sub> nanomaterials (A–C) and smaller size SnO<sub>2</sub> nano-assemblies (B–D) self-assembled to chain-like morphology in DNA.

N, and C. The intense Sn and O peaks came from the SnO<sub>2</sub> nano-assemblies while the N, P, and C peaks came from the DNA which is used during the synthesis and confirms its presence in the synthesized product. The Cl peak came from the Sn(II) chloride salt used during the synthesis. Fig. 4B shows the X-ray diffraction (XRD) pattern of the synthesized DNA–SnO<sub>2</sub> nano-assemblies after annealing the sample at 600 °C. Curves a and b indicate the XRD pattern of the DNA–SnO<sub>2</sub> chain-like morphology as having small size and large size particles. In both of the patterns, the diffraction peak originates from (110), (101), (200), (211), (220), (002), (310), (112), (202), (321), and (400) planes, respectively. The XRD was analyzed in the 2θ range from 10 to 90°. In both curves a and b we observed similar types of XRD patterns. All the above diffraction peaks match well with the standard data file of the SnO<sub>2</sub> having JCPDS file no. 41-1445 and can be straightforwardly indexed to the tetragonal rutile phase (*P4<sub>2</sub>/mnm*) of SnO<sub>2</sub>.<sup>35,36,41,42</sup> No peaks for the other phases of SnO<sub>2</sub> were detected, clearly indicating the high purity of the synthesized product. Wang *et al.* and Han *et al.* observed exactly similar types of XRD patterns from their synthesis of SnO<sub>2</sub> nanomaterials.<sup>35,41</sup>

### Photoluminescence (PL) study

Fig. 5 shows the room temperature photoluminescence (PL) emission spectra of the SnO<sub>2</sub> nano-assemblies. In PL, after light excitation by a photon, the electron hole pair might

recombine and the recombination rate is closely related to the electronic and the crystal structure. For SnO<sub>2</sub> nano-assemblies, the excitation spectrum (not shown here) was used to identify the excitation wavelength at which maximum emission takes place. From the excitation spectra it was found that, at an excitation wavelength of 230 nm, maximum emission takes place. Curve a and curve b in Fig. 5 show the PL emission spectra of chain-like SnO<sub>2</sub> nano-assemblies having large and small sizes, respectively. In both of these cases, we observed similar types of absorption spectra as expected. The emission bands are located at 426 nm, 487 nm and 521 nm, respectively. It was reported that SnO<sub>2</sub> thin films exhibited a broad dominant peak at 396 nm. In our study, all the emission maxima are located at a higher wavelength side compared to an earlier report by Gu *et al.*<sup>41</sup> signifying that the visible emission cannot be assigned to the direct recombination of a conduction electron in the Sn 4p band and a hole in the O 2p valance band. The highest intense peak at 426 nm might be due to the luminescence centers formed by such tin interstitials or from dangling in the SnO<sub>2</sub> nano-assemblies. The other emission band at the higher wavelength side at 487 nm and 521 nm is broad and less intense, probably due to electron transition mediated by defect levels in the band gap such as oxygen vacancies. So, we believe that, in our present SnO<sub>2</sub> nanomaterials, the intrinsic defects such as oxygen vacancy act as luminescence centers and can form defect levels located high



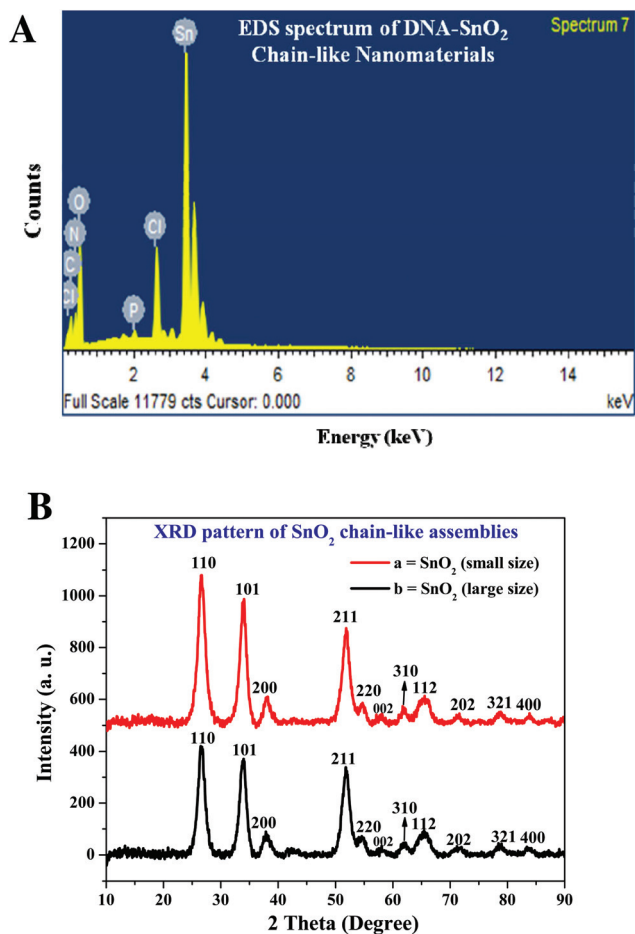


Fig. 4 (A) Energy dispersive X ray spectroscopy (EDS) analysis of DNA-SnO<sub>2</sub> nano-assemblies; the spectrum consists of peaks for Sn, O, P, N, Cl, and C. (B) X-ray diffraction (XRD) pattern of the two different morphologies (curve a, small size and curve b, large size) of the SnO<sub>2</sub> nano-assemblies with DNA respectively.

in the gap, trapping an electron from the valance band to make a contribution to the photoluminescence.

### Thermal analysis study

Fig. 6 shows the thermo gravimetric analysis (TGA) and differential thermal analysis (DTA) which are used to identify thermal stability and the crystalline condition of the DNA-SnO<sub>2</sub> nano-assemblies. The as-synthesized SnO<sub>2</sub> nano-assemblies were heated from RT to 1000 °C at a heating rate of 10 °C min<sup>-1</sup> and the experiment was performed at normal atmospheric conditions. Fig. 6, curve A indicates the TGA curve of SnO<sub>2</sub> nano-chains and curve B is the DTA curve of the same material. From the TGA curve we can see that a continuous weight loss takes place up to 291 °C and is due to loss of excess reagents or water molecules. A strong hump observed around 353 °C might be due to a phase change of the materials or due to conversion of Sn(OH)<sub>2</sub> to SnO<sub>2</sub>. After 353 °C, there was a gradual weight loss observed at 459 °C and 765 °C, which might be due to loss of excess DNA from the as-

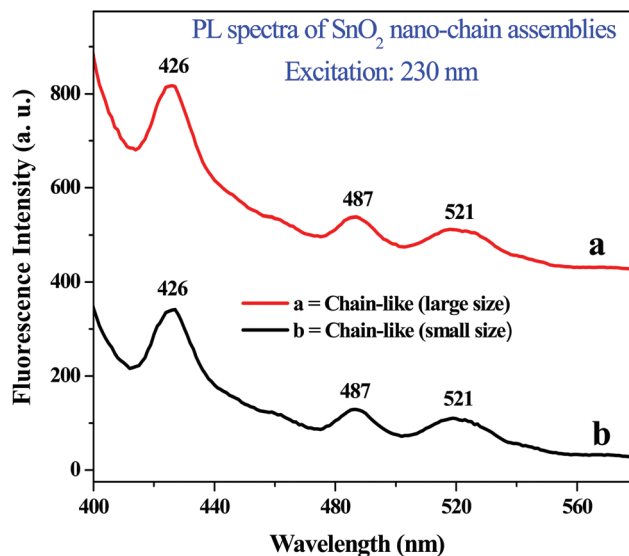


Fig. 5 The photoluminescence (PL) emission spectra of SnO<sub>2</sub> nano-assemblies on DNA with an excitation wavelength at 230 nm. Curve a and curve b indicate the emission spectra of chain-like SnO<sub>2</sub> nano-assemblies with large and small sizes, respectively.

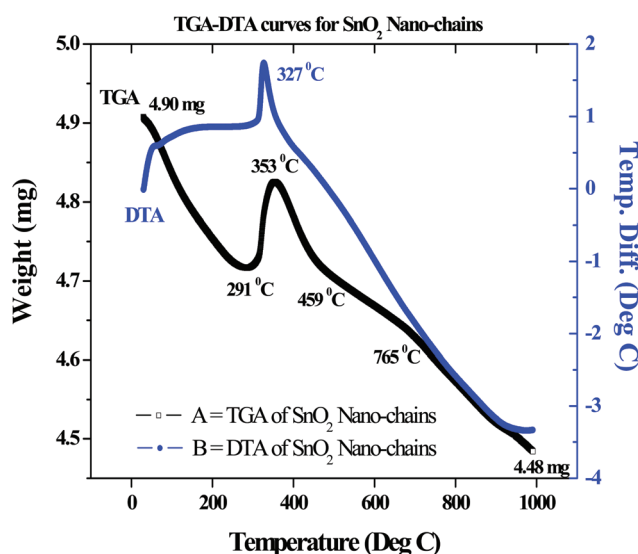


Fig. 6 The thermo gravimetric analysis (TGA) and differential thermal analysis (DTA) of the DNA-SnO<sub>2</sub> nano-assemblies where curve A indicates the TGA curve and curve B is the DTA curve, respectively.

synthesized DNA-SnO<sub>2</sub> samples. From the TGA curve, one can see that we started our experiment with 4.90 mg of sample and, after heating up to 1000 °C, the amount of sample retained was 4.48 mg. So the % of weight loss is ~8.58%. From the DTA curve in Fig. 6B, we can see one strong exotherm at 327 °C which might be due to phase change from amorphous to rutile phase. In our study, the as-synthesized DNA-SnO<sub>2</sub> nanomaterial was annealed at ~600 °C. We believe that DNA cannot be stable after thermal annealing at that high tempera-



ture; rather it might be denatured and all the nucleic acid bases should have been burnt off and been converted to meso/microporous carbon along with the N and P. However, initially during the synthesis, DNA served as a structure directing agent as well as a stabilizing agent for the formation of self-assembled SnO<sub>2</sub> nanomaterials. Karni *et al.*<sup>44</sup> investigated the stability of DNA with changes in temperature. They observed that under dry conditions, complete DNA degradation occurs at above 190 °C. Although in aqueous solution, the DNA degradation temperature will be a little higher as the boiling temperature of water is pressure dependent. Therefore, they investigated the thermal degradation of DNA in water for different applied partial pressures. Our TGA-DTA analyses found similarities with earlier reports where Nithiyantham *et al.* and Shek *et al.* observed similar types of TGA-DTA curves with the study of TiO<sub>2</sub> and SnO<sub>2</sub> nanomaterials.<sup>30,45</sup>

#### Fourier transform infrared (FT-IR) spectroscopic analysis

In our syntheses, we used DNA which provides a powerful means of rational assembly of nanomaterials. In DNA, a number of moieties and nucleotides, such as the backbone phosphate group and base functionalities, are potential candidates for terminating growth and serving as a capping layer. However, the salient chemical features of polynucleotides which are essential for the formation of chain-like SnO<sub>2</sub> nano-assemblies have not been identified yet. In an FT-IR study, we systematically investigated how the nucleotide functionalities influence NPs growth. Fig. 7 shows the FT-IR spectra where curve a is the spectrum for only DNA and curve b is the FT-IR spectrum for the SnO<sub>2</sub> nano-assemblies bound with DNA. Both the SnO<sub>2</sub> morphologies give similar types of FT-IR spectra, which are quite expected as both samples were pre-

pared using similar routes and bound by DNA only. The systematic and careful comparison between these two spectra not only indicated the presence of DNA on the SnO<sub>2</sub> surface, but also indicates the nature of the interaction taking place among them. In Curve a, in the case of only DNA, there are few low intense peaks that were observed at the lower wavenumber region of 490–660 cm<sup>-1</sup> and 700–1300 cm<sup>-1</sup> which are attributed to the stretching vibration of the P=O group in a DNA molecule. The specific peaks are either less intense or shifted in the case of DNA-bound SnO<sub>2</sub> samples and two strong peaks were observed at 706 cm<sup>-1</sup> and 1041 cm<sup>-1</sup>. The peak 1335–1820 cm<sup>-1</sup> is assigned to  $\nu(\text{C-O-X})$  mode where a sharp peak observed at 1633 cm<sup>-1</sup> for only DNA (curve a) and 1627 cm<sup>-1</sup> for the DNA bound SnO<sub>2</sub> sample (curve b). The specific shifting and presence of a peak at 1627 cm<sup>-1</sup> indicates the binding of SnO<sub>2</sub> nano-assemblies with DNA molecules. In both the samples a small intense but prominent peak is observed at 2326 cm<sup>-1</sup> which may be an overtone of some fundamental band. The stretching vibration appearing at the range of 2820–3000 cm<sup>-1</sup> indicates the stretching vibration of C-H bonds of a methylene group and the measured intensity directly indicated a change in the character of a particular band. The stretching vibration appeared at the wavenumber range 3200–3650 cm<sup>-1</sup> and indicates the -OH group. The -OH stretching appears at 3428 cm<sup>-1</sup> for only DNA and 3418 cm<sup>-1</sup> for a DNA bound SnO<sub>2</sub> sample. The shifting indicates the interaction of SnO<sub>2</sub> with the hydroxyl group present in a DNA molecule. A very high and strong intense peak is observed at 555 cm<sup>-1</sup> in the case of DNA bound SnO<sub>2</sub> which is absent for only a DNA sample; this signifies the characteristic absorption of antisymmetric Sn-O-Sn bonds due to presence of SnO<sub>2</sub> as reported before.<sup>29,41,46</sup> The specific P=O stretching bond at a lower wavenumber side for only DNA has been shifted and was much weaker in the case of DNA bound SnO<sub>2</sub> indicating the SnO<sub>2</sub> bonded with the phosphate group of DNA. The phosphate group might guide the interaction between DNA and Sn<sup>2+</sup> salt by electrostatic forces and tune the controlled growth of SnO<sub>2</sub> on a DNA molecule. Zhang *et al.* observed a peak at 615 cm<sup>-1</sup> from their study on a PANI/SnO<sub>2</sub> composite and assigned the peak for the anti-symmetric Sn-O-Sn mode of vibration.<sup>34</sup> Adnan *et al.* observed two bands at the lower wavenumber side at 667 cm<sup>-1</sup> and 554 cm<sup>-1</sup> which were attributed to the Sn-O stretching mode of Sn-O-Sn and Sn-OH, respectively.<sup>46</sup> They claimed that before calcinations not all the Sn(OH)<sub>4</sub> had undergone a condensation reaction to form SnO<sub>2</sub>. So, the above FT-IR analysis and literature study conclude that the phosphate back bone and sugar moiety present in DNA interact and help in binding SnO<sub>2</sub> particles with DNA. The specific FT-IR bands observed for our DNA, literature reported bands,<sup>41</sup> and the corresponding band assignments are summarized in Table 2.

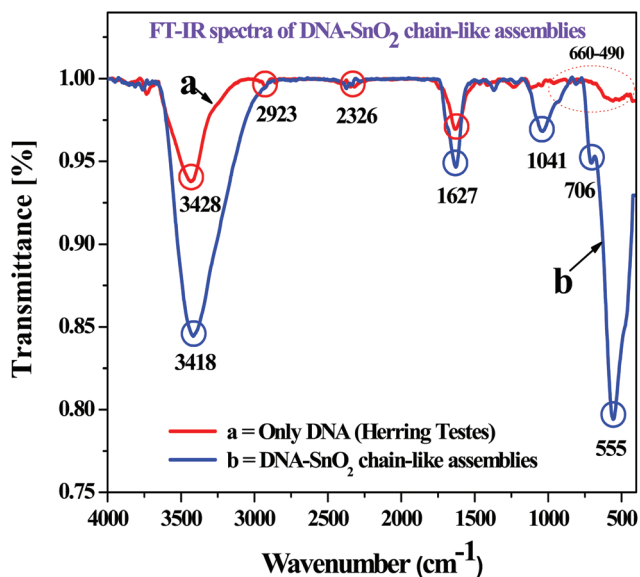


Fig. 7 The Fourier-transform infrared (FT-IR) spectra of bare DNA (curve a) and DNA bound SnO<sub>2</sub> nano-assemblies (curve b) at the wavenumber scale from 4000 to 400 cm<sup>-1</sup>.

#### Brunauer-Emmett-Teller (BET) analysis

The synthesized chain-like SnO<sub>2</sub> nano-assemblies are found to be suitable in electrochemical supercapacitors application for a potential anode material. The N<sub>2</sub> adsorption-desorption



**Table 2** The experimentally observed FT-IR bands of DNA, reported bands from literature, and the assignments of different peaks are summarized

Experimental and reported FT-IR bands for DNA		
FT-IR bands (cm <sup>-1</sup> ) (experimentally observed)	FT-IR frequency range (cm <sup>-1</sup> ) (reported value) <sup>46</sup>	Absorbing bonds/vibration types
3428	3100–3750	$\nu$ (OH group in DNA/water)
2923	2800–2950	Symmetric stretching vibration (C–H bonds in –CH <sub>2</sub> group)
1628	1732–1595	C=O, C–N, N–H <sup>46</sup>
—	1496–1480	Bending ( $\delta$ ) of C–H bond in CH <sub>2</sub>
1235	1170–1300	Asymmetric stretching of PO <sub>2</sub> <sup>-</sup> group
1115	1150–990	$\nu$ (C–O–C, C–C) <sup>46</sup>
490–660	400–1000	De-oxyribose region

isotherm *via* BET surface area measurements taking small size (curve a) and large size (curve b) SnO<sub>2</sub> chain-like nano-assemblies are shown in Fig. 8. From Fig. 8, the specific surface area (SSA) of the small size chain-like SnO<sub>2</sub> nano-assemblies were calculated from the BET analysis, which is 163.2 m<sup>2</sup> g<sup>-1</sup>. The specific pore size distribution is favorable for improving the electrochemical behavior in a small size SnO<sub>2</sub> nano-assembly electrode due to the unhindered diffusion and accession of electrolyte ions into the inner space/matrix. The BET SSA for large size chain-like SnO<sub>2</sub> nano-assemblies is calculated to be 145.6 m<sup>2</sup> g<sup>-1</sup>.

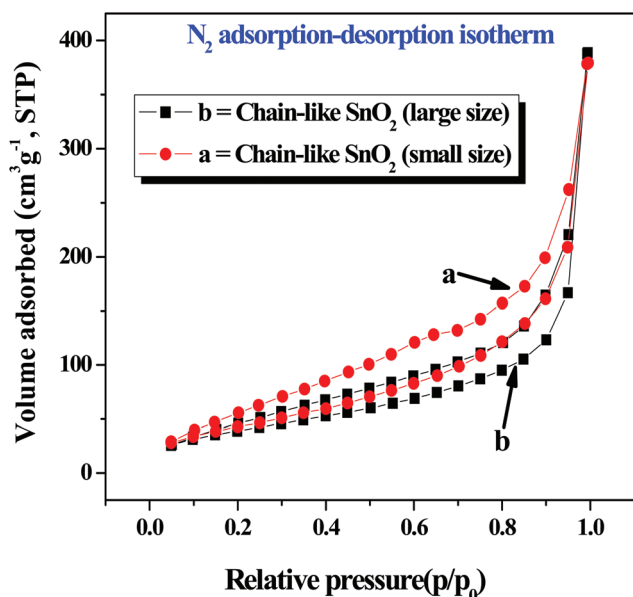
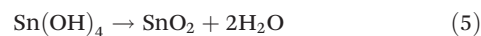
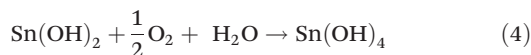
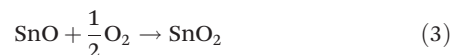
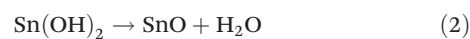
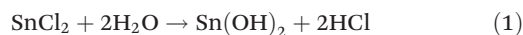


**Fig. 8** The N<sub>2</sub> adsorption–desorption isotherm *via* BET surface area measurements with small size (curve a) and large size (curve b) chain-like SnO<sub>2</sub> nano-assemblies.

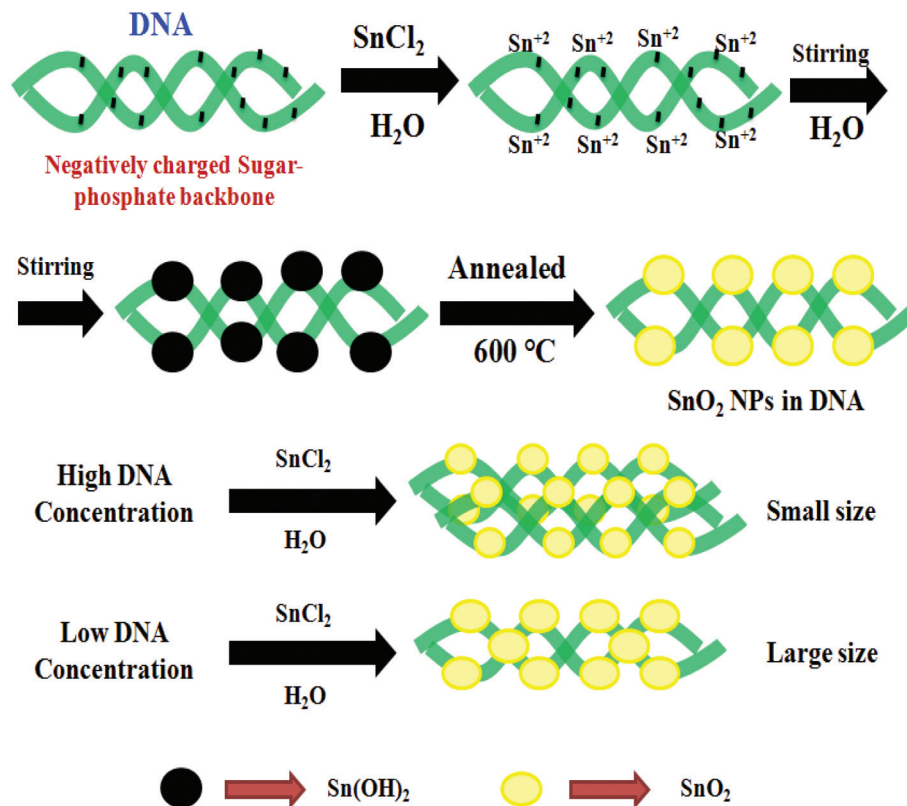
## Reaction mechanisms for the formation of chain-like SnO<sub>2</sub> nano-assemblies

Self-assembled, aggregated chain-like SnO<sub>2</sub> nano-assemblies were synthesized by the reaction of Sn(II) chloride salt in aqueous solution in the presence of a DNA scaffold under continuous stirring at room temperature. Two different morphologies of SnO<sub>2</sub> nano-chains were formed by varying the starting reagent concentration as given in Table 1. In our synthesis, we have seen that the presence of DNA is extremely important for the generation of chain-like SnO<sub>2</sub> nano-assemblies. By keeping the other reaction conditions the same, just in the absence of DNA, only aggregated humps of nano-assemblies without any specific morphology were formed. We believe that the presence of DNA in our synthesis not only acts as a scaffold or stabilizing agent, but also directs the nucleation and growth of the SnO<sub>2</sub> particles in a specific crystallographic direction and generate the chain-like morphology. In our synthesis, we used tin(II) chloride as a precursor salt for tin; it is a colorless liquid in ethanol and light white color in water and rapidly soluble in both solvents, having a density of 2.71 g cc<sup>-1</sup> and 3.95 g cc<sup>-1</sup> in dehydrate and anhydrous conditions, respectively. It has a melting point of 247 °C and boiling point of 623 °C. In the presence of DNA and water, Sn(II) is oxidized to Sn(IV) which is necessary for the formation of SnO<sub>2</sub> nano-assemblies. The probable chemical reaction takes place as follows.



So, during the formation of SnO<sub>2</sub>, different intermediate products like SnO, Sn(OH)<sub>2</sub>, and Sn(OH)<sub>4</sub> are formed and then finally dehydration and oxidation take place and generate the SnO<sub>2</sub> nano-assemblies. Rogach *et al.* also proposed similar types of reaction mechanisms for the formation of hierarchical SnO<sub>2</sub> nano-assemblies. Scheme 2 shows the schematic formation of SnO<sub>2</sub> nano-chains on a DNA scaffold. From this scheme, we can see that initially after the addition of Sn<sup>2+</sup> ions in aqueous DNA solution, Sn<sup>2+</sup> attached on a DNA due to electrostatic interaction of the oppositely charged ions. Now, under a stirring condition in aqueous solution, Sn<sup>2+</sup> ions gets hydrated and produces Sn(OH)<sub>2</sub> and finally, after annealing the sample at 600 °C, it generates SnO<sub>2</sub> which binds with the DNA scaffold and forms the chain-like morphology. The phosphate and hydroxyl groups present in DNA primarily guide the interaction of the DNA chain with Sn<sup>2+</sup> ions and helps the controlled growth of SnO<sub>2</sub> particles on DNA to a chain-like morphology. From the FT-IR analyses, as discussed before, we have already seen that the phosphate and hydroxyl groups are





**Scheme 2** Formation mechanism for the synthesis of chain-like SnO<sub>2</sub> nano-assemblies on a DNA scaffold.

responsible for the binding of Sn<sup>2+</sup> ions with DNA and they formed the chain-like SnO<sub>2</sub> nano-assemblies. From Scheme 2, we can see that, at high DNA concentration or at lower DNA concentration, in both the cases, chain-like SnO<sub>2</sub> nano-assemblies are formed although the individual particles size and chain diameter varies with respect to the DNA concentration. We have seen that, at a high DNA concentration, the individual SnO<sub>2</sub> particles are formed in smaller size compared to lower DNA concentration, due to restricted growth of the particles at high DNA concentration. In a lower DNA concentration, the pre-formed SnO<sub>2</sub> particles do not grow in any specific direction due to less restriction on their growth, and generate the larger diameter particles. Similar types of restricted growth and different size particle formation was reported by others.<sup>30,47</sup> In the formation of TiO<sub>2</sub> nano-assemblies on DNA, it was observed that P=O and C-O-P groups can be adsorbed on the surface of the oxide nano-assemblies by simple chemical adsorption.<sup>37</sup> So all the above and previous analyses show that DNA offered a negatively charged phosphate backbone for the attaching sites to localize the inorganic metal complexes. This novel combination has yielded similar responsive chain-like nano-assemblies. Once SnO<sub>2</sub> nuclei are formed by dehydration and oxidation of the Sn(OH)<sub>2</sub>, they grow and once the size reaches a critical value they form the SnO<sub>2</sub> NPs. The SnO<sub>2</sub> NPs grow along the DNA chain and self-assembled, aggregated together to form the chain-like nano-assembly. Similar types of a formation mechanism were elaborated by Gao *et al.* for

the formation of a chain-like ZnO assembly on DNA.<sup>48</sup> At this point, the detailed formation mechanism is premature although it is reasonable to assume that a DNA phosphate back bone and hydroxyl moieties might guide the SnO<sub>2</sub> particles to grow in a specific direction and generate the chain-like morphology. Taking the chain-like SnO<sub>2</sub> nano-assemblies, we have studied their application in electrochemical supercapacitor as discussed below.

#### Electrochemical supercapacitor application of the chain-like SnO<sub>2</sub> nano-assemblies

The electrochemical properties of the as-prepared chain-like small and large size SnO<sub>2</sub> electrodes were evaluated by cyclic voltammetry, galvanostatic charge/discharge, and electrochemical impedance spectroscopy measurements in 2 M KOH aqueous solution as the electrolyte. Fig. 9a shows the CV curves for the chain-like small (a-1) and large (b-1) size SnO<sub>2</sub> electrodes at 5 mV s<sup>-1</sup>. It can be seen that the electrodes exhibited well-define redox peaks in anodic and cathodic sweeps, which indicates that the SnO<sub>2</sub> electrodes were mainly governed by a redox mechanism. Compared to larger sized SnO<sub>2</sub>, the smaller sized SnO<sub>2</sub> electrode showed increased current intensity, which indicates the higher specific capacitance of the electrode material. Fig. 9b and c display the CV curves of chain-like small and large size SnO<sub>2</sub> electrodes at scan rates of 5, 10, 20, 40, 60, and 80 mV s<sup>-1</sup>. It can be seen that all the CV curves exhibited a similar shape of anodic and



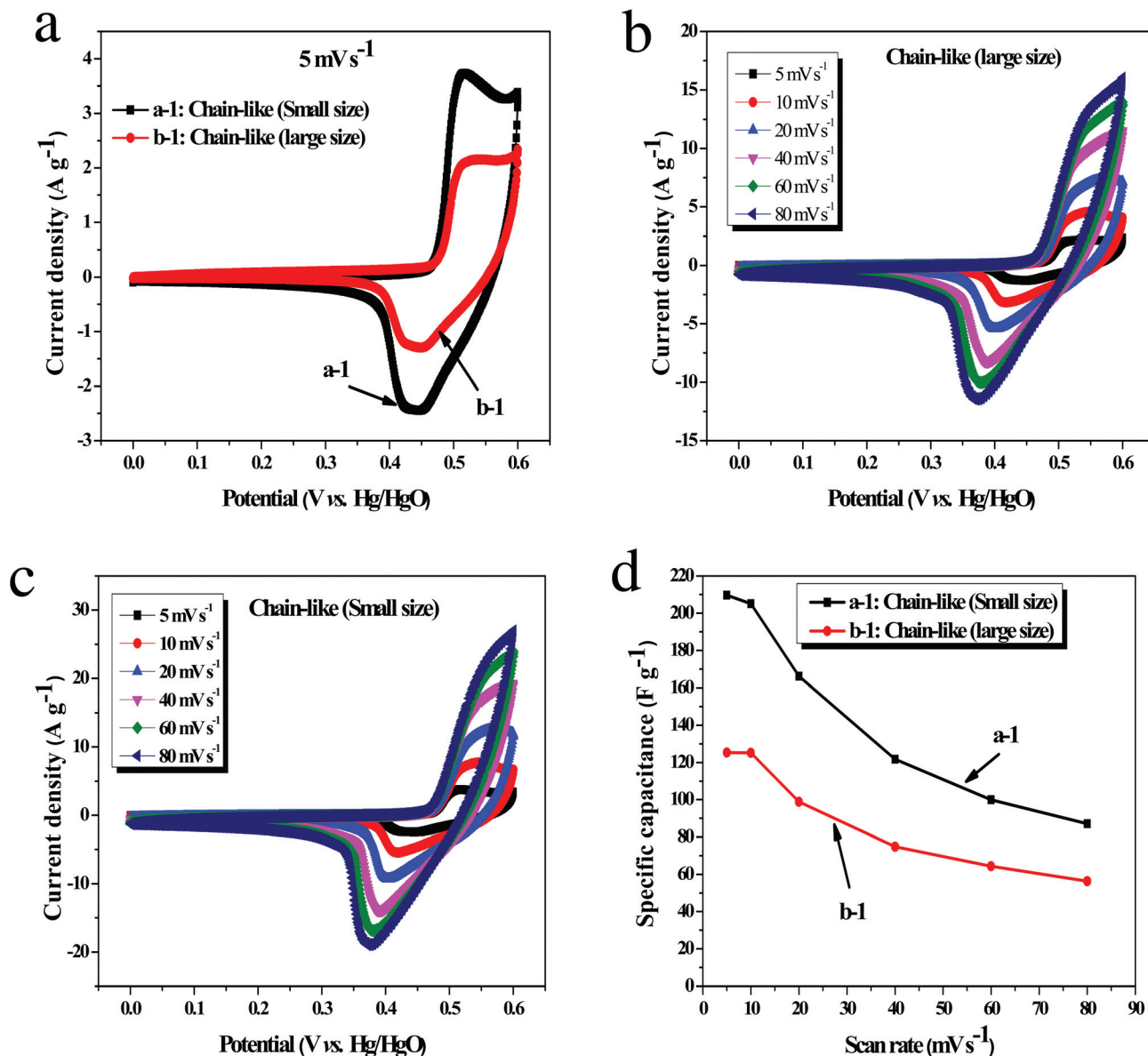


Fig. 9 (a) Cyclic voltammetry curve of chain-like small (a-1) and large (b-1) size SnO<sub>2</sub> electrodes in 2 M KOH electrolyte at a scan rate 5 mV s<sup>-1</sup>. Cyclic voltammetry curve of chain-like small (b) and large (c) size SnO<sub>2</sub> electrodes at different scan rates. (d) Specific capacitance as a function of scan rate for chain-like small (a-1) and large (b-1) size SnO<sub>2</sub> electrodes.

cathodic peaks with rising scan rates, indicating good reversibility of the redox reaction at the interface of a nanostructure and good rate capability. In addition, the anodic and cathodic peaks were shifted towards the positive and negative potential with increasing the scan rates, which is mainly due to the rate of mass transfer limitations of electrolyte ions in order to neutralize the electronic charge on the electrode surface during the redox reaction.<sup>49,50</sup> Fig. 9d shows the specific capacitance as a function of scan rate for chain-like small (a-1) and large (b-1) size SnO<sub>2</sub> electrodes. The specific capacitance of the chain-like small and large size SnO<sub>2</sub> calculated from the CV curves (eqn (1)) were 209 and 126 F g<sup>-1</sup> at a scan rate of 5 mV s<sup>-1</sup> and 87 and 56 F g<sup>-1</sup> at a high scan rate of 80 mV s<sup>-1</sup>. Also, it can

be found that the specific capacitance of small and large size SnO<sub>2</sub> electrodes obtained at a higher scan rate of 80 mV s<sup>-1</sup> still preserved 42 and 44% of its initial specific capacitance value obtained at 5 mV s<sup>-1</sup>, which indicates the good rate capability of the fabricated electrode. With increasing scan rates, the specific capacitance decreases gradually because the redox reaction is diffusion limited. At a low scan rate, the electrolyte ions could possibly diffuse (allow more time for the electrolyte ions to access the whole surface) into both the inner and outer surface of the electroactive material for energy storage, whereas with increasing scan rate, only the outer surface was utilized for charge storage due to insufficient time available for ion diffusion at the inner surface of the nanostructure.<sup>51–53</sup>



The electrochemical properties of as-prepared electrodes were further examined by a galvanostatic charge/discharge test. Fig. 10a compares the GCD curves of chain-like small (a-1) and large (b-1) size SnO<sub>2</sub> electrodes at a current density of 0.5 A g<sup>-1</sup>. The non-linear charge/discharge curves and the distinct voltage plateaus of the as-prepared SnO<sub>2</sub> electrodes match well with the CV results, which further confirms the pseudocapacitive behavior of the SnO<sub>2</sub>. As expected, the small size SnO<sub>2</sub> electrodes exhibited a longer discharge time than the larger size SnO<sub>2</sub>, demonstrating their higher capacitance. The GCD measurements were further conducted at various current densities. As shown in Fig. 10b and c, the curves exhibited a similar shape with a voltage plateau, further

confirming the pseudocapacitive behavior of the electroactive materials. According to the GCD curves, the specific capacitance of the small and large size SnO<sub>2</sub> electrodes can be calculated by using eqn (2). The specific capacitance *versus* current density is plotted in Fig. 10d. The specific capacitance of the small (a-1) and large (b-1) size SnO<sub>2</sub> electrode is 151 and 100 F g<sup>-1</sup> at 0.5 A g<sup>-1</sup>, respectively. Even as the current density increases to 7.5 A g<sup>-1</sup>, the small and large size SnO<sub>2</sub> electrodes still retain 54 and 43% of their initial specific capacitance (0.5 A g<sup>-1</sup>), which indicates the better rate capability of the as-prepared electrodes. Compared to the large size electrode, the smaller size SnO<sub>2</sub> electrode revealed higher capacitance. Also, the obtained specific capacitance (151 at 0.5 A g<sup>-1</sup>; 209 at

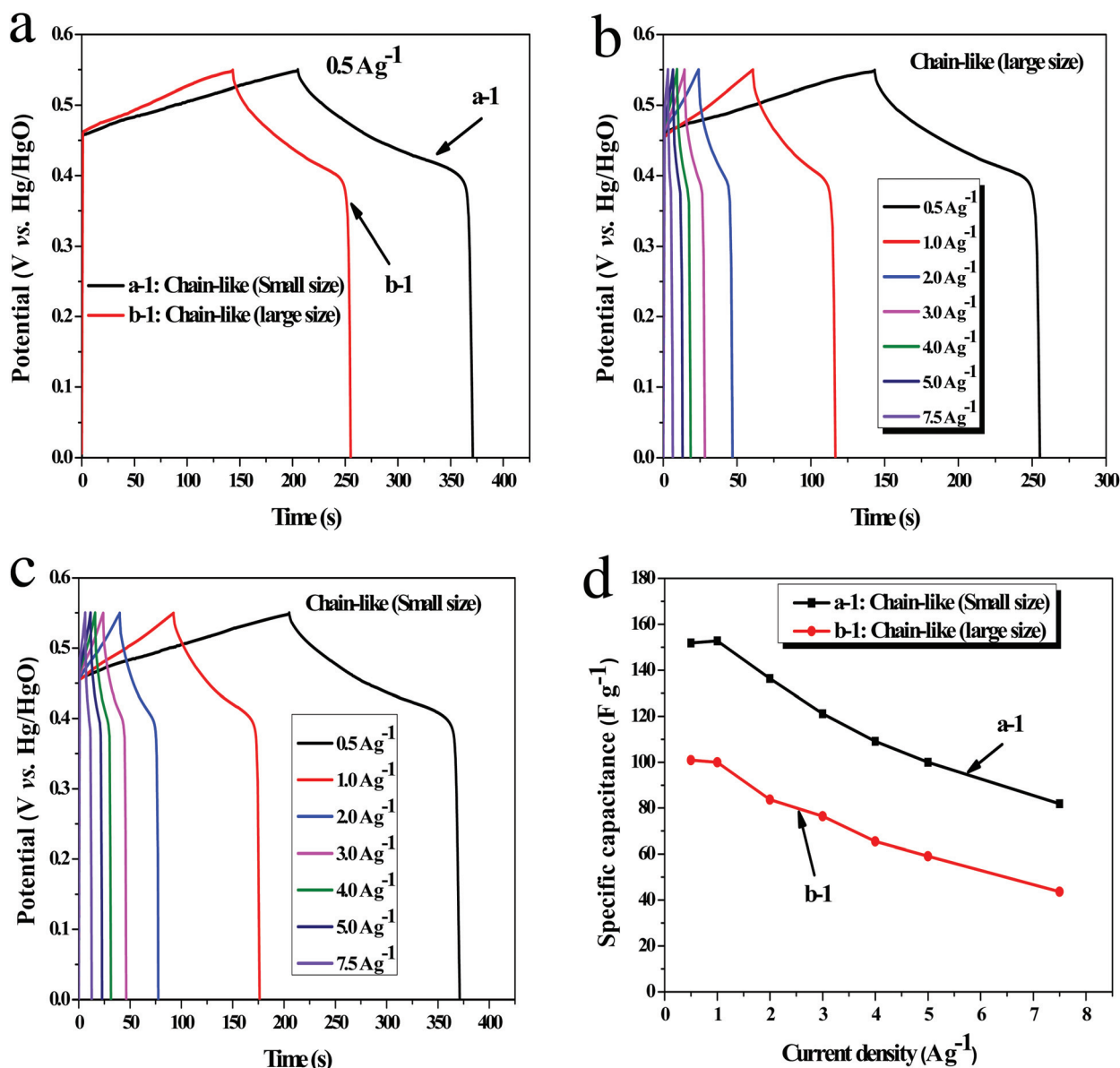


Fig. 10 (a) Galvanostatic charge/discharge curves of chain-like small (a-1) and large (b-1) size SnO<sub>2</sub> electrodes. GCD curves of chain-like small (b) and large (c) size SnO<sub>2</sub> electrodes. (d) Specific capacitance for chain-like small (a-1) and large (b-1) size SnO<sub>2</sub> electrodes.



$5 \text{ mV s}^{-1}$ ) of the smaller size  $\text{SnO}_2$  electrode is higher than the previously reported  $\text{SnO}_2$  supercapacitor.<sup>54–57</sup> From BET analysis as discussed before, we observed that the surface area of chain-like  $\text{SnO}_2$  nano-assemblies having small size are  $\sim 163.2 \text{ (m}^2 \text{ g}^{-1}\text{)}$  and having large size  $\sim 145.6 \text{ (m}^2 \text{ g}^{-1}\text{)}$ . The enhanced capacitance of the smaller particle size  $\text{SnO}_2$  electrode can be attributed to the higher surface area which provides numerous sites for faradaic reaction and also the

smaller size particles reduce the diffusion path length for easy access of ions/electron in to the porous structure.

In order to further evaluate the electronic conductivity of the as-prepared  $\text{SnO}_2$  electrodes, an EIS measurement was performed. Fig. 11a depicts the Nyquist plots of chain-like small and large size  $\text{SnO}_2$  electrodes. The Nyquist plots exhibited a semicircle arc in the high frequency region and a slope of a straight line in the low frequency region. Further, it can be

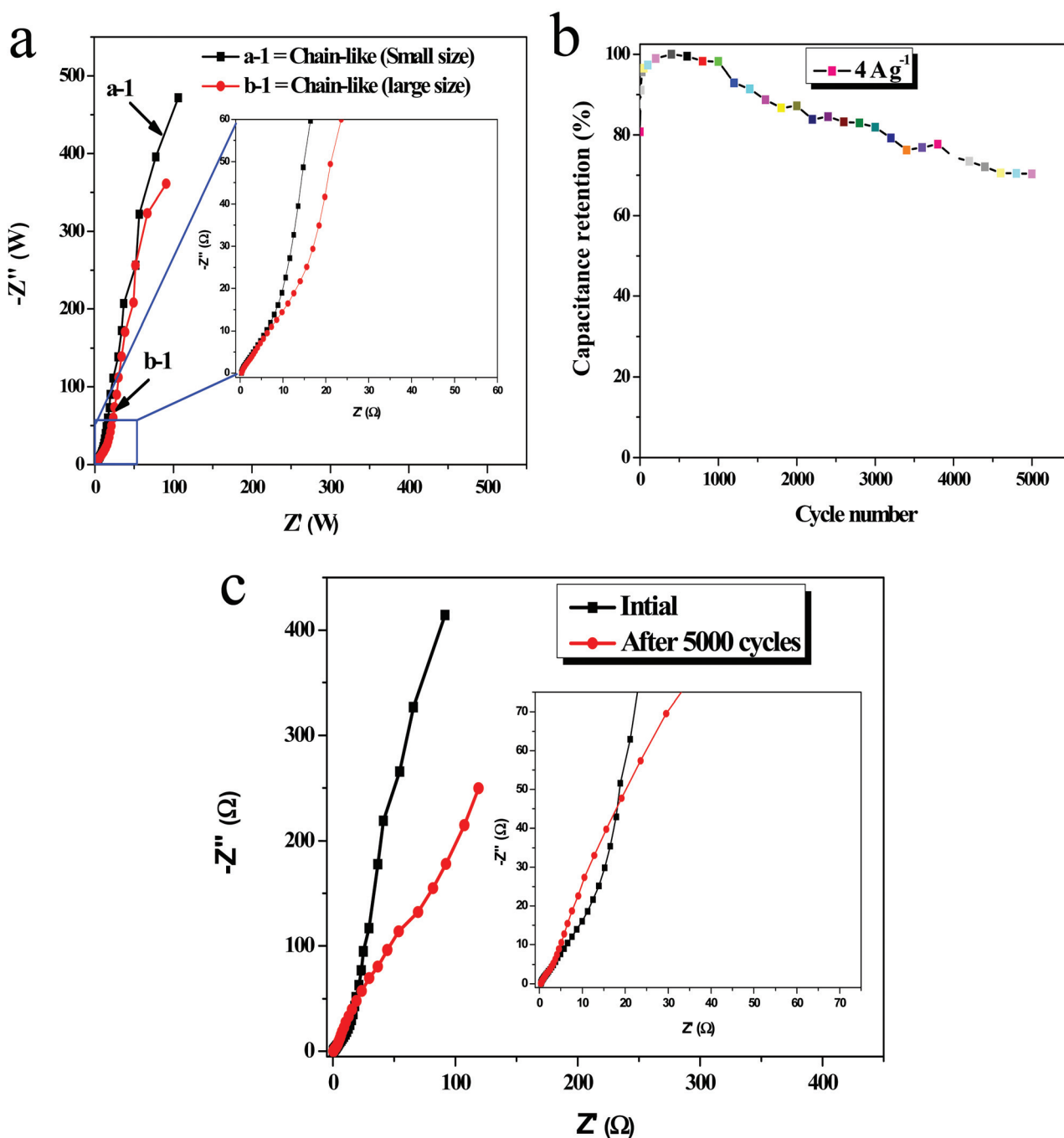


**Fig. 11** (a) Nyquist plots of chain-like small and large size  $\text{SnO}_2$  electrodes. Inset is the magnified portion. (b) Cyclic stability of small size  $\text{SnO}_2$  electrodes at  $4 \text{ A g}^{-1}$  for 5000 cycles. (c) Nyquist plots of small size  $\text{SnO}_2$  electrode before and after 5000 cycling tests.



seen that both electrode plots were similar with a semicircle and a straight line. The intercept on the  $Z$  real axis and a semicircle arc at the high frequency region indicate the solution resistance ( $R_s$ ) and charge transfer resistance ( $R_{ct}$ ), respectively. The charge transfer resistance of the as-prepared chain-like small ( $R_s = 0.29 \Omega$ ) and large ( $R_s = 0.35 \Omega$ ) size SnO<sub>2</sub> electrodes were estimated as 10.3  $\Omega$  and 16.6  $\Omega$ . Compared to the large sized SnO<sub>2</sub> electrode, the small sized SnO<sub>2</sub> electrode revealed a smaller solution resistance and reduced charge transfer resistance, which indicates better electronic conductivity. This may be due to the small size of SnO<sub>2</sub>, which reduced the ion/electron pathway. Moreover, a straight line slope at low frequency indicates low diffusion resistance and good capacitive behavior of the electrode.

Long-term cycling stability is an important parameter to evaluate the practical application of supercapacitors. The cycling stability of the small size SnO<sub>2</sub> electrode was evaluated by repeating the charge/discharge measurement at a constant high current density of 4 A g<sup>-1</sup> for 5000 cycles. Fig. 11b shows the variation of specific capacitance *versus* cycle number. It can be seen that the specific capacitance of the electrodes gradually increased for the first 500 cycles, which is ascribed to the activation process of the electroactive materials.<sup>58</sup> Then the specific capacitance slightly decreased and retained 71% of the capacitance even after 5000 cycles, which demonstrated the better cycling stability of the electrode material. In order to further understand the cycling stability and fundamental behavior of the small size SnO<sub>2</sub> electrode, we performed EIS analysis before and after the long term cycle test. Fig. 11c shows the Nyquist plots of the small size SnO<sub>2</sub> electrode before and after 5000 cycling tests. It can be seen that the Nyquist plots consist of a semicircle arc and a straight line at the high- and low-frequency regions, respectively. Noticeably, the charge-transfer resistance of the electrodes after 5000 cycles was slightly decreased, which may be due to the electro-activation process by repetitive charge/discharge cycles. The higher charge-transfer resistance before the cycling test is attributed to the usage of binder to prepare the working electrode, which inhibits the easy access of electrolyte ions into the inner surface of electroactive materials for the first few hundred cycles. After continuous a cycling process, the electrode becomes accessible to whole active areas. But, the straight line at the low-frequency region is slightly inclined towards the real axis after 5000 cycles, which indicates that the diffusive resistance of the electrode increased and caused the decreases in specific capacitance.

## Conclusion

In conclusion, two different morphologies of self-assembled, aggregated, chain-like SnO<sub>2</sub> nano-assemblies were synthesized at room temperature by utilizing a simple wet chemical route in under a one hour reaction time. Smaller size and larger size SnO<sub>2</sub> nano-chains were formed by controlling the DNA to Sn(II) ions molar ratio and by tuning the other reaction parameters. Different analytical and spectroscopic tools were used for

measuring the materials size, shape, and morphology. The probable reaction mechanism for the formation and growth of the SnO<sub>2</sub> NPs on DNA is discussed. The SnO<sub>2</sub> chain-like nano-assemblies were utilized as electrode materials in an electrochemical supercapacitor study. From the supercapacitor study, it was found that the SnO<sub>2</sub> nanomaterials showed different specific capacitance ( $C_s$ ) values for the various chain-like morphologies and the order of  $C_s$  values are as follows: chain-like (small size) > chain-like (large size). The highest  $C_s$  of 209 F g<sup>-1</sup> at a scan rate of 5 mV s<sup>-1</sup> was observed for SnO<sub>2</sub> having a chain-like structure with small sizes. A long term cycling stability study of a chain-like SnO<sub>2</sub> electrode showed it to be stable and retaining *ca.* 71% of the initial specific capacitance, even after 5000 cycles. From the supercapacitor study, it was seen that both of the morphologies can be used as potential anode materials and a reasonable efficiency was observed with the SnO<sub>2</sub> having small size chain-like morphology due to their high BET surface area and specific structural orientation. Our present route provides an easy way to fabricate SnO<sub>2</sub> chain-like nano-assemblies by virtue of its simplicity and environmentally benign nature, which makes them a promising candidate for further processing, assembly, and practical application with other oxide based nanostructures.

## Acknowledgements

S K and U N wishes to acknowledge Dr V. K. Pillai, Director and Dr M. Jayachandran, HOD, ECMS Division, CSIR-CECRI for their support and encouragement. We wish to acknowledge Mr S. R. Ede, JRF, CSIR-CECRI for help during the entire experiment. The research funding from Molecules to Materials to Devices (M2D) program, CSC0134, by CSIR, New Delhi and DST, SERB, New Delhi (DST Fast Track project No # SR/FT/CS-98/2011, GAP 7/12), support from the Central Instrumental Facility (CIF) and help from Mr A. Rathishkumar and R Prabu (TEM and FE-SEM in-charge, CIF) CSIR-CECRI are appreciated.

## References

- 1 Y. Zhang, T. Ichihashi, E. Landree, F. Nihey and S. Iijima, *Science*, 1999, **285**, 1719.
- 2 H. J. Dai, E. W. Wong, Y. Z. Lu, S. S. Fan and C. M. Lieber, *Nature*, 1995, **375**, 769.
- 3 F. Gyger, M. Hubner, C. Feldmann, N. Barsan and U. Weimar, *Chem. Mater.*, 2010, **22**, 4821.
- 4 A. Kay and M. Grätzel, *Chem. Mater.*, 2002, **14**, 2930.
- 5 H. J. Snaith and C. Ducati, *Nano Lett.*, 2010, **10**, 1259.
- 6 H. Zhang and C. Hu, *Catal. Commun.*, 2011, **14**, 32.
- 7 S. Ding, J. S. Chen and X. W. Lou, *Adv. Funct. Mater.*, 2011, **21**, 4120.
- 8 F. L. Chen and M. L. Liu, *Chem. Commun.*, 1999, 1829.
- 9 X. Xu, J. Zhuang and X. Wang, *J. Am. Chem. Soc.*, 2008, **130**, 12527.



- 10 D. F. Zhang, L. D. Sun, J. L. Yin and C. H. Yan, *Adv. Mater.*, 2003, **15**, 1022.
- 11 Z. W. Pan, Z. R. Dai and Z. L. Wang, *Science*, 2001, **291**, 1947.
- 12 Y. Wang, X. Jiang and Y. Xia, *J. Am. Chem. Soc.*, 2003, **125**, 16176.
- 13 Y. Wang, H. C. Zeng and J. Y. Lee, *Adv. Mater.*, 2006, **18**, 645.
- 14 C. Wang, Y. Zhou, M. Ge, X. Xu, Z. Zhang and J. Z. Jiang, *J. Am. Chem. Soc.*, 2009, **132**, 46.
- 15 J. Gong, G. Li and Z. Tang, *Nano Today*, 2012, **7**, 564.
- 16 Y. Gao and Z. Tang, *Small*, 2011, **7**, 2133.
- 17 S. W. Lee, C. B. Mao, C. E. Flynn and A. M. Belcher, *Science*, 2002, **296**, 892.
- 18 R. A. Mcmillan, C. D. Paavola, J. Howard, N. J. Zaluzec and J. D. Trent, *Nat. Mater.*, 2002, **1**, 247.
- 19 T. Scheibel, R. Parthasarathy, G. Sawicki, X. M. Lin, H. Jaeger and S. L. Lindquist, *Proc. Natl. Acad. Sci. U. S. A.*, 2003, **100**, 4527.
- 20 S. Kundu and H. Liang, *Adv. Mater.*, 2008, **20**, 826.
- 21 S. Kundu and H. Liang, *Langmuir*, 2008, **24**, 9668.
- 22 D. Majumdar, A. Singha, P. K. Mondal and S. Kundu, *ACS Appl. Mater. Interfaces*, 2013, **5**, 7798.
- 23 U. Nithyanantham, S. R. Ede and S. Kundu, *J. Mater. Chem. C*, 2014, **2**, 3782.
- 24 S. Kundu, K. Wang, D. Huitink and H. Liang, *Langmuir*, 2009, **25**, 10146.
- 25 N. C. Seeman, *Curr. Opin. Struct. Biol.*, 1996, **6**, 519.
- 26 J. Zhang, Y. Liu, Y. Ke and H. Yan, *Nano Lett.*, 2006, **6**, 248.
- 27 M. C. SanMartin, C. Gruss and J. M. Carazo, *J. Mol. Biol.*, 1997, **268**, 15.
- 28 E. Braun, Y. Eichen and U. Sivan, *Nature*, 1998, **391**, 775.
- 29 S. R. Ede, A. Ramdoss, S. Anantharaj, U. Nithyanantham and S. Kundu, *Phys. Chem. Chem. Phys.*, 2014, **16**, 21846.
- 30 U. Nithyanantham, A. Ramdoss, S. R. Ede and S. Kundu, *Nanoscale*, 2014, **6**, 8010.
- 31 C.-C. Hu, K.-H. Chang, M. C. Lin and Y.-T. Wu, *Nano Lett.*, 2006, **6**, 2690.
- 32 S. Gubbala, V. Chakrapani, V. Kumar and M. K. Sunkara, *Adv. Funct. Mater.*, 2008, **18**, 2411.
- 33 A. Thapa, J. Zai, H. Elbohy, P. Poudel, N. Adhikari, X. Qian and Q. Qiao, *Nano Res.*, 2014, **7**, 1154.
- 34 Z.-A. Hu, Y.-L. Xie, Y.-X. Wang, L.-P. Mo, Y.-Y. Yang and Z.-Y. Zhang, *Mater. Chem. Phys.*, 2009, **114**, 990.
- 35 Y.-L. Wang, M. Guo, M. Zhang and X.-D. Wang, *CrystEngComm*, 2010, **12**, 4024.
- 36 C. Gao, X. Li, B. Lu, L. Chen, Y. Wang, F. Teng, J. Wang, Z. Zhang, X. Pan and E. Xie, *Nanoscale*, 2012, **4**, 3475.
- 37 A. Birkel, Y.-G. Lee, D. Koll, X. V. Meerbeek, S. Frank, M. J. Choi, Y. S. Kang, K. Char and W. Tremel, *Energy Environ. Sci.*, 2012, **5**, 5392.
- 38 C. Prasittichai and J. T. Hupp, *J. Phys. Chem. Lett.*, 2010, **1**, 1611.
- 39 H. Zhang and C. Hu, *Catal. Commun.*, 2011, **14**, 32.
- 40 Y. Song, X. Cai, X. Xu and X.-X. Liu, *J. Mater. Chem. A*, 2015, **3**, 14712.
- 41 F. Gu, S. F. Wang, C. F. Song, M. K. Lu, Y. X. Qi, G. J. Zhou, D. Xu and D. R. Yuan, *Chem. Phys. Lett.*, 2003, **372**, 451.
- 42 Y. Han, X. Wu, Y. Ma, L. Gong, F. Qu and H. Fan, *CrystEngComm*, 2011, **13**, 3506.
- 43 S. Kundu, N. Sutradhar, R. Thangamuthu, B. Subramanian, A. B. Panda and M. Jayachandran, *J. Nanopart. Res.*, 2012, **14**, 1040.
- 44 M. Karni, D. Zidon, P. Polak, Z. Zalevsky and O. Shefi, *DNA Cell Biol.*, 2013, **32**, 1.
- 45 C. H. Shek and G. M. Lin, *J. Mater. Res.*, 2000, **15**, 1994.
- 46 M. A. Farrukh, B.-T. Heng and R. Adnan, *Turk. J. Chem.*, 2010, **34**, 537.
- 47 U. Nithyanantham, S. R. Ede, S. Anantharaj and S. Kundu, *Cryst. Growth Des.*, 2015, **15**, 673.
- 48 N. Li, Y. Gao, L. Hou and F. Gao, *J. Phys. Chem. C*, 2011, **115**, 25266.
- 49 X. Li, X. Xiong, J. Li, J. Bai and Y. Qian, *J. Mater. Chem.*, 2012, **22**, 14276.
- 50 F. I. Dar, K. R. Moonoswamy and M. E. Souni, *Nanoscale Res. Lett.*, 2013, **8**, 363.
- 51 A. Ramadoss, B. Saravanakumar and S. J. Kim, *Energy Technol.*, 2015, **3**, 913.
- 52 A. Ramadoss and S. J. Kim, *Electrochim. Acta*, 2014, **136**, 105.
- 53 S. K. Balasingam, J. S. Lee and Y. Jun, *Dalton Trans.*, 2015, **44**, 15491.
- 54 Y. Liu, Y. Jiao, Z. Zhang, F. Qu, A. Umar and X. Wu, *ACS Appl. Mater. Interfaces*, 2014, **6**, 2174.
- 55 N. L. Wu, *Mater. Chem. Phys.*, 2002, **75**, 6.
- 56 R. KalaiSelvan, I. Perelshtein, N. Perkas and A. Gedanken, *J. Phys. Chem. C*, 2008, **112**, 1825.
- 57 F. Li, J. Song, H. Yang, S. Gan, Q. Zhang, D. Han, A. Ivaska and L. Niu, *Nanotechnology*, 2009, **20**, 455602–455601.
- 58 J. Pu, J. Wang, X. Jin, F. Cui, E. Sheng and Z. Wang, *Electrochim. Acta*, 2013, **106**, 226.

